Materials Advances

ROYAL SOCIETY OF CHEMISTRY

PAPER

View Article Online
View Journal | View Issue

Cite this: *Mater. Adv.*, 2025, **6**, 4738

Enhanced properties of bamboo short fiber reinforced polymer composites with alkali and graphene oxide

Md. Ariful Islam, *[a] Mainul Islam,[a] Md. Shariful Islam[a] and Tarikul Islam *[bc]

Bamboo short fibers (BSFs) have become popular as sustainable alternatives to synthetic fibers because of their present affordable performance levels and environmentally friendly solutions. The main challenge with bamboo fiber composites is their weak interfacial bonding and insufficient mechanical strength. This research investigated mechanical and interfacial performance optimization of BSFs by applying alkali treatment and graphene oxide (GO) coating methods. The alkali treatment successfully eliminated non-cellulosic contaminants and strengthened the bond between fiber and matrix, and then the sequential GO coating operation brought additional reinforcing benefits to the system. Various tests analyzed the prepared composites, including tensile, flexural, impact, hardness, FTIR, DMA, TGA, water absorption, and SEM analyses. The tensile strength of alkali-treated and GO-coated BSFs composites surpassed untreated fibers by ~113%, and their flexural strength achieved ~93% increase. Impact resistance also improved significantly. Definitive signs point to the modified BSFs having potential as high-performance, environmentally sustainable reinforcements for polymer composites because of their strengthened interface bond and improved thermal stability. The study brings forward valuable information for developing sustainable composite materials that can serve structural needs and industrial processing demands.

Received 20th February 2025,
Accepted 27th May 2025

DOI: 10.1039/d5ma00158g

rsc.li/materials-advances

1. Introduction

The rising environmental concerns, declining fossil fuel supplies, and changing climate patterns have elevated the interest in using natural plant fibers to substitute synthetic fibers in polymeric composites. The market has recently exhibited considerable interest in utilizing plant fibers consisting of jute, bamboo, coir, flax, hemp, banana, kenaf, sisal, *etc*. Plant-based fibers are more popular among researchers because they present low density, better thermal insulating performance, and impressive mechanical properties.[1,2] Natural plant fibers constitute an excellent substitute for synthetic fibers because they offer affordability and longevity while being environmentally sustainable and biodegradable. Sustainability-compatible performance features and cost-effectiveness make these materials attractive worldwide as solutions to current environmental protection issues. Manufacturers in various industries use these fibers as appropriate replacements for synthetic fibers when producing automobiles, together with aerospace equipment, and constructing buildings.[3,4]

Bamboo is the most significant natural fiber plant due to its incredibly fast growth rate and wide range of applications.[1] Bamboo is important as a basic material for green product development because it exhibits versatility, durability, and quick regenerative capabilities. Bamboo and natural plant fibers will thrive as sustainable solutions because the world seeks environmentally friendly approaches to reducing both fossil fuel consumption and synthetic material pollution of our ecosystems.[5] The extraction of bamboo fibers starts by processing bamboo culm using various methods such as mechanical procedures, chemical procedures, and integrated chemical-mechanical methods.[6] Extracted bamboo fibers undergo a combination of compression molding with roller mills, following their treatment with chemicals that remove the remaining materials.[7] The bamboo culm contains three types of tissues, which distribute their components as fibers, taking up 40%, and parenchyma, carrying 50%, with conductive tissue occupying the remaining 10%.[5,7,8] Two types of cells comprise bamboo culm parenchyma tissue, which has significant importance because long parenchyma cells display thick poly lamellate lignified walls while short parenchyma cells exhibit thin unlignified walls.[5,9]

[a] *Department of Textile Engineering, Dhaka University of Engineering and Technology, Gazipur 1707, Bangladesh. E-mail: arifulislam@duet.ac.bd*
[b] *Department of Textiles, Merchandising, and Interiors, University of Georgia, Athens, Georgia 30602, USA. E-mail: tarikul@uga.edu*
[c] *Department of Textile Engineering, Jashore University of Science and Technology, Jashore 7408, Bangladesh*

These parenchyma cells adhere to bamboo fiber surfaces, which contributes to its complete structure and characteristics. The bamboo fibers contain primarily three lignocellulosic components, which are cellulose, hemicellulose, and lignin.[9] The lengthwise bamboo fibers stay directed for full culm extension to give these materials outstanding tensile strength.[10] The bamboo culm extracts show fiber bundles extending 20 to 35 cm while maintaining diameters between 90 and 280 μm.[4] Most bamboo fiber weight comes from cellulose, hemicellulose, and lignin, which amount to more than 90%, with smaller amounts of soluble polysaccharides, waxes, and ashes.[11,12] When viewed across their sections, bamboo fiber bundles consist of rod-shaped elementary units between hexagonal and pentagonal shapes. Bamboo fibers exist in dimensions between 10 to 40 micrometers in diameter, whereas their sizes range from 1.0 to 4.3 millimeters in length.[4] The unique structure of bamboo fibers enhances their strength and flexibility while promoting sustainability, which allows them to succeed, especially in eco-friendly product development and composites. The use of bamboo fiber-based unidirectional (UD) plant-based composites becomes prevalent in mechanically demanding applications because UD preforms provide higher load-bearing capacity.[13] Strength-wise, UD-based preforms deliver good results, but weak resin infiltration leads to diminished fiber–matrix interface and impaired composite engineering properties.[13,14] Bamboo fiber production requires substantial energy usage, resulting in mechanical damage to the fibers.[15,16] However, there is a problem with the UD composite, as its transverse strength is low.[17] The development of innovative bamboo fiber preforms requires attention because they must show exceptional mechanical performance despite a reduced number of manufacturing operations. The integration of this method would protect fibers from damage and cut production expenses while lowering resource requirements and production waste. The development of more efficient bamboo-based composite materials requires optimized bamboo fiber utilization in simplified processing systems. The approach serves sustainability targets and enhances both the mechanical properties of the composites. Technical bamboo fiber elasticity exists between 19 and 43 GPa, and tensile strength spans between 341 and 860 MPa, while growth conditions and species influence these properties.[4] According to research, the hydrophilic quality of bamboo fibers produces poor bonding with hydrophobic polymer matrices, which deteriorates the mechanical composite properties.[18,19] The mechanical performance of bamboo fibers is negatively affected by hemicellulose and lignin because they cause reduced fiber crystallinity, according to a literature study.[20,21] Improvement of fiber–matrix bonding for specific applications is achieved when bamboo fibers receive chemical treatments to reach the required mechanical properties. Research shows that alkali treatment is a simple yet effective method for improving the bond between fibers and matrices.[22–26] One of the most frequently used methods for alkali treatment involves sodium hydroxide (NaOH) solutions and effective methods for surface-treating bamboo fiber bundles, enhancing both their physical and mechanical properties.[27]

Previous researchers have reported that alkali treatment improves natural fiber–polymer interface adhesion and simultaneously results in superior physical attributes, mechanical properties, and elevated thermal features.[28–30] When applying alkali treatment, the primary process involves dissolving hemicellulose and lignin components from within the fiber structure so that bamboo fibrils become a rougher surface and decentralized.[20,31] The surface area of the fiber increases through this treatment, making the polymer matrix able to bond better with interface.[32] Thicker contact opportunities between the polymer and surface improve the interface bonding with the fiber material. Through alkali treatment, the chemical activity of bamboo fibers is enhanced as the treatment breaks cellulose chain hydrogen bonds and raises the concentration of surface hydroxyl groups.[32,33] Strong bonding results from the enlarged fiber affinity toward the polymer matrix, which stems from the higher density of hydroxyl groups accessible on its surface. The surface of the treated fibers develops higher roughness, which leads to improved mechanical locking between the fiber–matrix elements, which strengthens the composite interphase.[33–36] Multiple improved interfacial effects between the bamboo fiber and polymer matrix create a stronger bond that results in superior composite material performance.[34] Research indicates that GO becomes an effective coating material due to its numerous superior properties, including high mechanical strength, thermal stability, and exceptional barrier function.[37] Applying GO to bamboo fiber results in fibers that exhibit improved water resistance, thermal stability, and mechanical properties, expanding their potential applications.[38]

The two-dimensional material commonly known as graphene consists only of carbon atoms because it uses a completely carbon-atom structure.[39] The production of graphene nanoplatelets starts with intercalating and exfoliating natural graphite before performing strong oxidation to obtain GO. The hydrophilic nature and chemical reactivity of GO sheets arise from oxygen-bearing functional groups consisting of hydroxyl groups, epoxide, carbonyl, and carboxyl groups.[39–41] The oxygen-containing functional groups allow GO to become hydrophilic, to disperse nicely in water, and enable efficient functionalization. The approximately 1 μm lateral dimension of GO sheets makes them easily compatible with polymer matrices to boost the performance characteristics of composites.[42] Its functional groups facilitate effective chemical bonding and homogenous matrix dispersion, which positions GO as a superior choice for reinforcing composite materials while enhancing property performance.[42,43]

Research has shown that adding GO and GO-derived graphene materials as composite fillers significantly enhances the mechanical performance, electrical conductivity, and thermal stability of polymer composites. Experimental evidence indicates that GO and its derived graphene serve as excellent filler materials for creating composites with improved multifunctional properties.[44–47] The incorporation of 0.7 wt% GO to Young's modulus increases by 62% while tensile strength improved by 76%.[48] The effective load transfer mechanism between GO sheets and the polymer matrix improves both stress distribution and structural integrity, enabling further enhancements.[48,49]

Many studies show that GO coatings improve synthetic fiber property behavior, which results in improved mechanical efficiency and enhanced interfacial contact throughout composite materials.[48–52] When GO sheets became part of carbon fiber-reinforced epoxy composite sizing agents, they produced substantial tensile performance gains alongside enhanced interfacial shear strength by 71%.[53,54] High-quality surface bonding between the GO coating and short carbon fibers led to increased tensile strength that surpassed untreated controls by 12 percent, according to research findings.[55] The incorporation of GO into glass fabric/epoxy composites caused a 33% enhancement in interlaminar shear strength, which demonstrates GO's effectiveness in enhancing fiber–matrix attachments.[56] Laboratory tests have validated the effectiveness of covalent GO attachment to glass fibers because it reinforces both interfacial regions and overall material performance.[57] When scientists applied alkali treatment to jute fibers, leading to GO coating at different concentrations between 0.25 to 1 wt%, researchers achieved better Young's modulus, tensile strength, and interfacial shear strength in epoxy matrix composites *versus* non-treated fibers.[21] Recently, surface modification on natural fibers using nanostructured materials has attracted considerable attention due to their biocompatibility and ability to develop significant interfacial interactions due to several reactive sites.[58–61] Such treatments are potentially beneficial for the adhesion between fiber and matrix to improve the stability and compatibility of natural fiber composites.[60] However, some works have presented the grafting of nanoparticles such as NanoTiO$_2$ and ZnO$_2$ onto natural fibers.[62,63] The effect of alkali treatment and graphene or its derivatives as coating in natural short fibers has not been studied. Studies have not been conducted on this dual-modification strategy applied to common natural random short fibers such as bamboo, thus indicating an important gap in the field and its application in material-rich composite development.

This study addresses the challenge of weak interfacial bonding in bamboo short fiber composites by introducing an integrated approach that combines chemical surface modification and nanoscale reinforcement of bamboo short fiber (BSF) preforms. BSFs were treated with an alkali to enhance fiber–matrix compatibility and subsequently purified. Then, the surface modification of the GO coating was implemented to improve the interfacial adhesion and mechanical properties. The modified BSFs were then converted into dry preforms, which were used to prepare bamboo/epoxy-based composites through conventional molding methods. Mechanical properties of the prepared composites were systematically assessed through tensile, flexural, impact, and hardness tests, and thermal and structural properties were characterized using FTIR, DMA, TGA, water absorption experiments, and SEM of fractured surfaces. This suggests that the synergism of employing alkali treatment and GO coating can greatly improve the mechanical strength, stiffness, durability, and thermal stability of the composite. Finally, through extensive characterization, the mechanical and sustainability performance of the developed BSF composites was compared with synthetic fiber-reinforced composites, elucidating the merit potential of BSF composites as high-performance structural applications.

2. Experimental Methods

2.1. Materials

Bamboo (*Bambusa Vulgaris*) fibers (approximately 20–25 cm) were collected from a local market near Gazipur, Bangladesh, and were extracted by mechanical methods. The supplier has submitted a comprehensive list of properties (see Fig. 1 and Table 1). Graphene oxide (GO) was synthesized from graphite powder, which was collected from the Institute of Atomic Energy Research Establishment (AERE), Savar, Dhaka. Sodium hydroxide (NaOH), sulfuric acid (H_2SO_4), potassium permanganate ($KMnO_4$), hydrochloric acid (HCl), and sodium nitrate ($NaNO_3$), Hydrogen peroxide (H_2O_2) were also used for GO synthesis, NaOH was used for fiber treatment, epoxy resin, and amine hardener were used for composite preparation. All laboratory reagent-grade chemicals were purchased from Jonaki Scientific House, Dhaka, Bangladesh, and used without further conditioning or purification.

2.2. Methodology

2.2.1. Fiber individualization and preparation for different short fiber lengths. Raw bamboo fibers were rinsed several times with deionized water (DI) and then dried at 80 °C for 1 hour before use. The fibers were initially individualized using a hand-combing tool. The fibers were then carefully cut into four different lengths: 5 mm, 10 mm, 15 mm, and 20 mm, using scissors (see Fig. 2).

2.2.2. Graphene oxide synthesis process. Graphene oxide (GO) was synthesized using a modified Hummers' method.[64] Graphite powder was mixed with potassium permanganate and sulfuric acid in a reaction vessel. The mixture was stirred and maintained below 20 °C to prevent overheating. The strong oxidizing agents oxidized the graphite, incorporating oxygen-containing functional groups into the graphene structure. Post-reaction, the experiment received an addition of hydrogen peroxide solution to both stop the oxidation process and counteract extra permanganate ions. The mixture was then washed with water and treated with ethanol. This wash removed acids, salts, and unreacted reagents. Finally, GO was separated by filtration from the liquid phase (see Fig. 3).

2.2.3. BSFs treated with alkali. Table 2 lists the different fiber treatments and their corresponding codes. Raw bamboo fibers without chemical applications underwent no treatment before different fiber lengths were optimized. Once the optimal fiber length of 5 mm was determined, chemical treatments were applied exclusively to the cut fibers of this optimized length. The fibers were immersed in a 5 wt% NaOH solution at a 1 : 30 liquor ratio for 1 hour at 100 °C for alkali treatment.[65] After the treatment, the fibers were thoroughly rinsed with deionized water until the pH reached a neutral level.

2.2.4. BSFs coated with GO. To apply the GO coating, the alkali-treated fibers were immersed in a 1 wt% GO solution for 30 minutes, followed by a drying process to remove moisture from the fibers.[66] Both the alkali treatment and GO coating were performed before the preform manufacturing process (see Fig. 4).

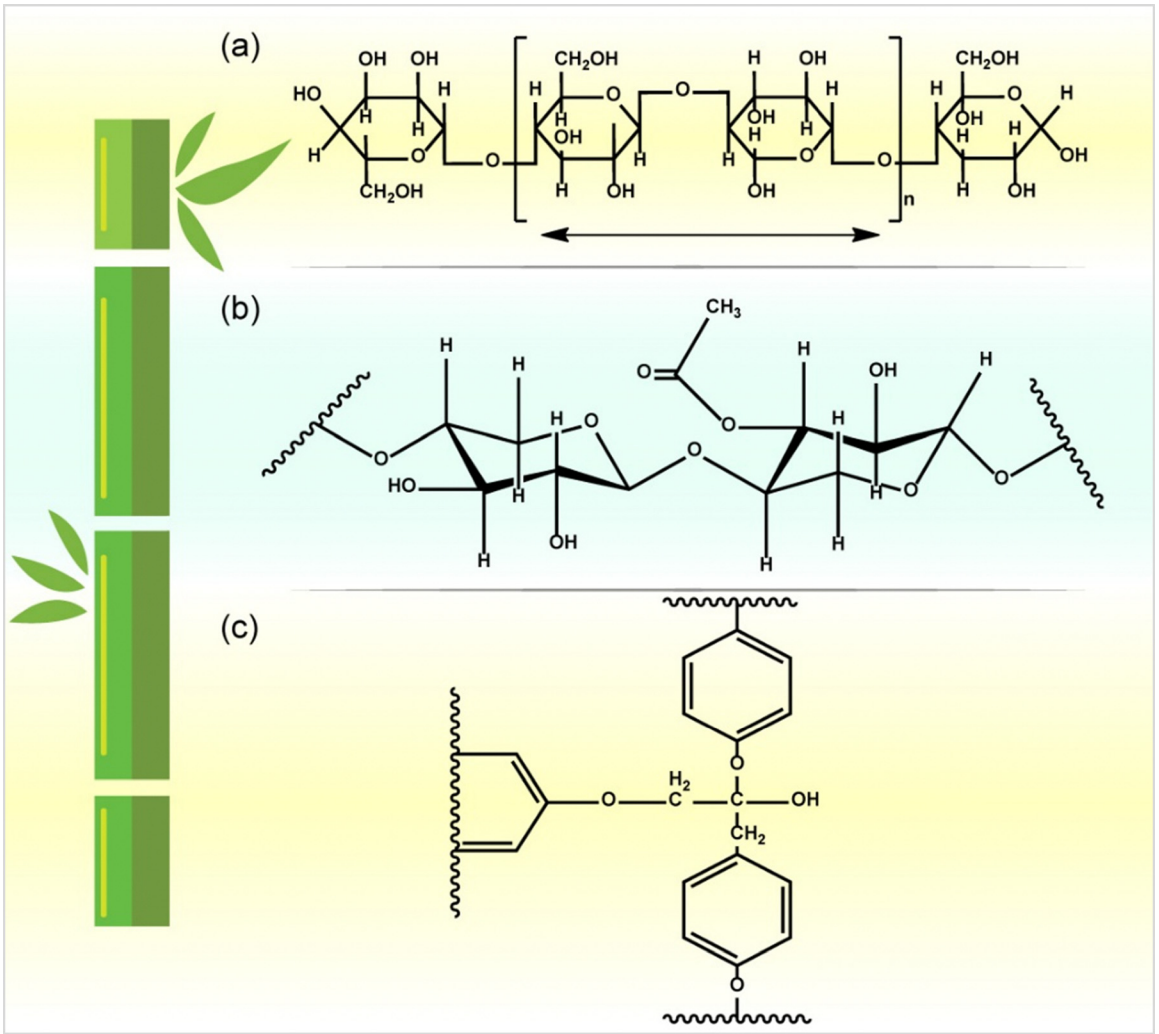

Fig. 1 Chemical structures of bamboo (a) cellulose, (b) hemicellulose, and (c) lignin.

Table 1 Properties of BSFs

Material	Tensile modulus (GPa)	Tensile strength (MPa)	Density (g cm^{-3})	Specific modulus (GPa g^{-1} cm^{-3})	Specific strength (MPa g^{-1} cm^{-3})	Failure stain (%)
BSFs	38	665	1.5	21.33	315	1.13

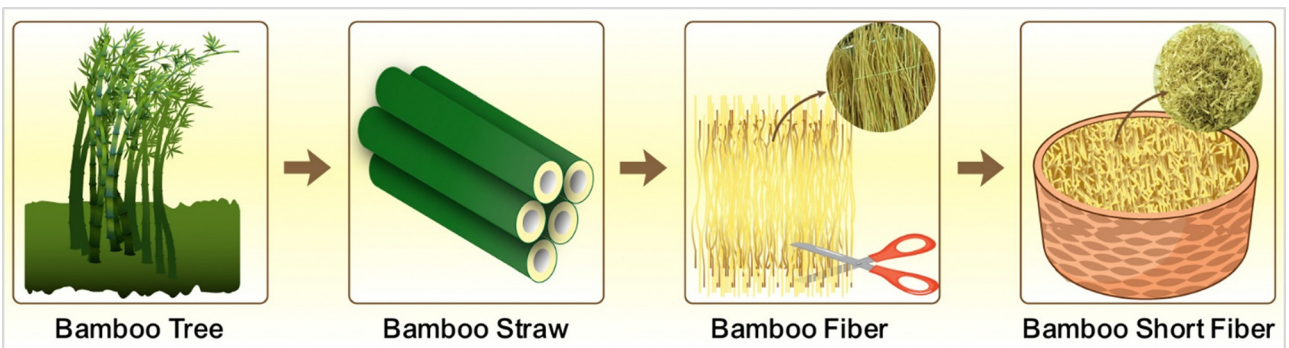

Fig. 2 Bamboo short fiber preparation process.

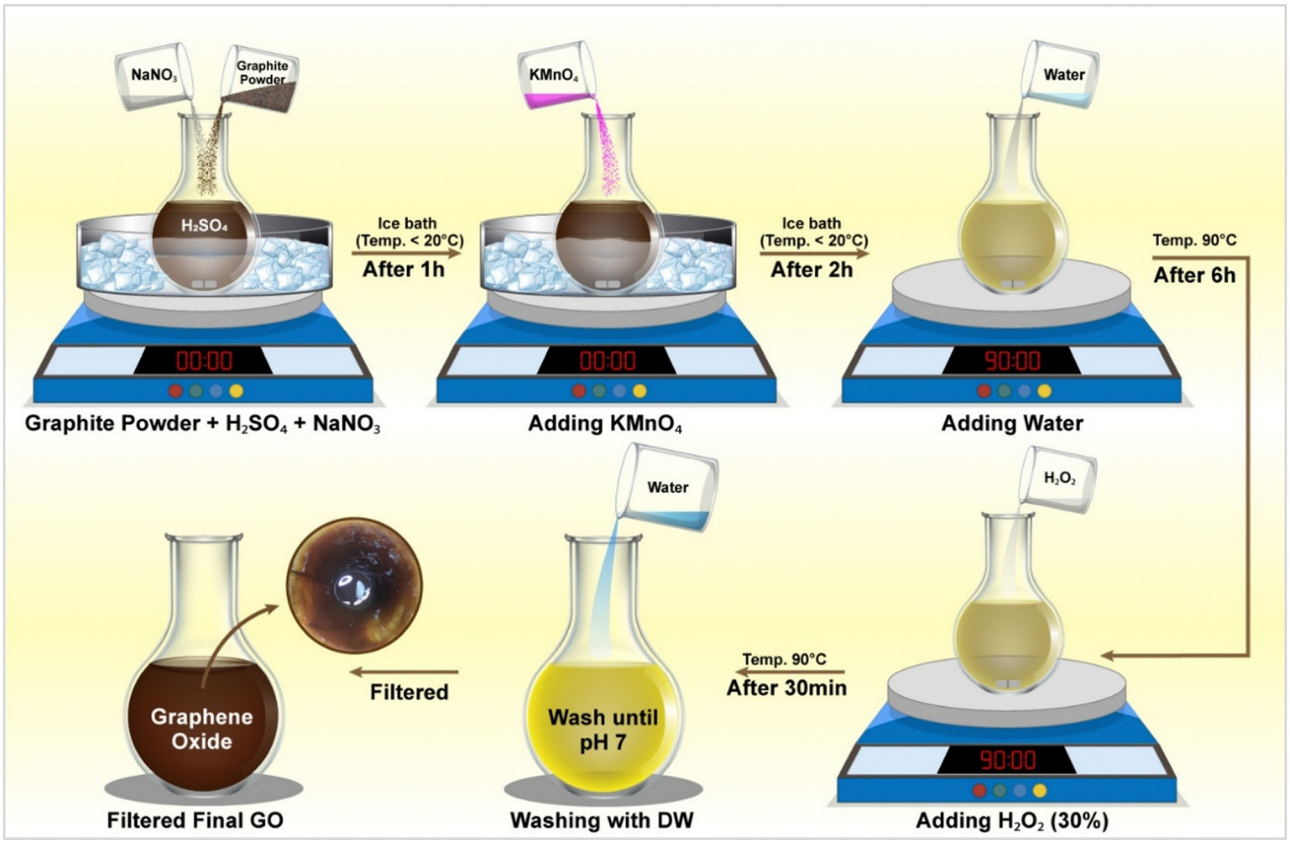

Fig. 3 Synthesis process of graphene oxide from graphite powder.

Table 2 Different fiber lengths and treated composites and their coding

No.	Name	Code
1	Raw bamboo fiber with 5 mm length	UTB5
2	Raw bamboo fiber with 10 mm length	UTB10
3	Raw bamboo fiber with 15 mm length	UTB15
4	Raw bamboo fiber with 20 mm length	UTB20
5	5% alkali treatment of UTB5 fibers	ATB
6	ATB dip-coated in 1 wt% GO solution	AGB

2.2.5. Preform manufacturing of BSFs. Short bamboo fiber-based dry preforms were produced using fibers of varying lengths (UTB5, UTB10, UTB20, and UTB15) with and without chemical treatments. The process began by placing the cut fibers into a steel square box, which was then submerged in a metal bowl containing deionized water. The box, perforated at the bottom, allowed water to flow through while keeping the fibers contained. The fibers were thoroughly wetted by stirring, and the metal bowl was heated to approximately 80 $\pm$ 5 °C to enhance the interaction between the water and fibers. After 30 minutes, a fiber cake formed inside the box (see Fig. 4). The wet fiber cakes were transferred to rectangular metal frames (200 mm $\times$ 200 mm $\times$ 3 mm), where water was squeezed out through compression in a molding machine. The frames were pressed at 120 °C with 1 ton per square inch force for at least 30 minutes to dry and compress the fibers into preforms. For alkali-treated and GO-coated fiber-based preforms, the treatment

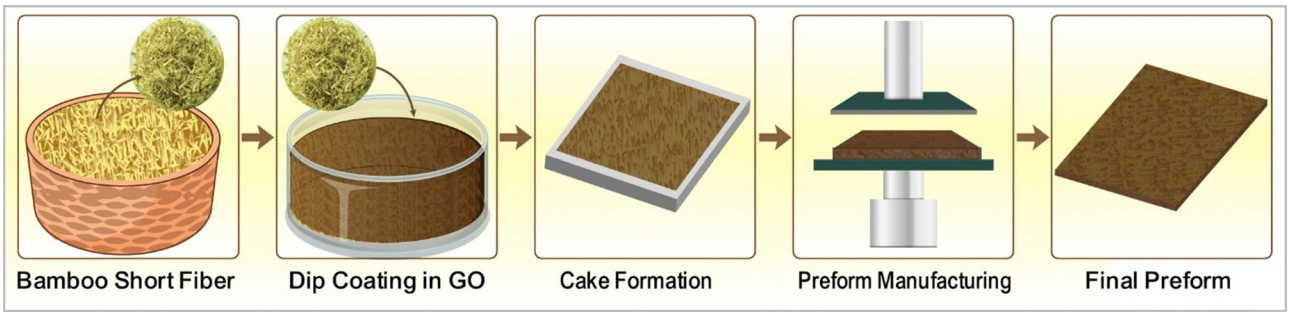

Fig. 4 BSFs GO coating and dry preform manufacturing process.

Table 3 Physical dimensions of developed preforms

Preforms	Preform size (mm)	Preform thickness (mm)	Areal density (GSM)
UTB5	200 × 200	2.93 ± 0.23	1735 ± 112
UTB10	200 × 200	2.98 ± 0.35	1762 ± 116
UTB15	200 × 200	3.01 ± 0.24	1795 ± 109
UTB20	200 × 200	2.94 ± 0.18	1773 ± 114
ATB	200 × 200	3.12 ± 0.13	1812 ± 120
AGB	200 × 200	3.05 ± 0.18	1795 ± 118

and coating were applied prior to the preform manufacturing. This process resulted in highly packed, uniform, and high-performance bamboo fiber dry preforms, as shown in Fig. 4. The physical properties of the preforms are detailed in Table 3.

2.2.6. Composite manufacturing. The composites were produced using a compression molding technique combined with rapid-curing epoxy resin (see Fig. 5). All types of composites were manufactured under identical conditions. The dry fiber preforms were initially placed in an oven for 4 hours to decrease the moisture content. Hardener was mixed with the epoxy resin at a 1 : 10 ratio. This mixture was applied to both sides of the preforms using the brush (see Fig. 5a). Teflon sheets were placed on the top and bottom of the wet preform layup, which was then placed between the upper and lower metal plates of the compression molding machine. A high pressure of 1 ton was applied for 30 minutes at a temperature of 70 °C. After the molding process, the composites were removed from the machine and kept to cool to room temperature (see Fig. 5b–d).

2.3. Characterization

2.3.1. Tensile test. The tests followed ASTM D 638-03 procedure using an AG-X Plus Universal Testing Machine (Japan) with a 20 kN load cell. The dimensions of the specimens were 165 mm long, 20 mm wide, and 3 mm thick. During the test, the testing machine operated at a constant crosshead speed of 1 mm min^{-1}. The experiment included testing three samples of each composite type to achieve dependable results. Each specimen underwent testing to determine its tensile strength, which resulted in mean calculation alongside standard deviation for data validation purposes.

2.3.2. Flexural test. For the flexural test, the Universal Testing Machine AG-X Plus was operated using a three-point bending procedure according to ASTM D 790. Scientists prepared samples from the specimens by cutting them into 125 mm lengths and 20 mm widths with a thickness of 3 mm. The testing area between supports was established at 50 mm while the machine operated at 1.4 mm min^{-1} crosshead speed. The flexural strength and modulus evaluation of each composite type utilized no less than five testing specimens. Testing of the hybrid composites through this process revealed important information about their bending characteristics. The laboratory testing of the samples relied on three-point bending analysis through the application of eqn (1).

$$L = (D + 3a) \pm a/2 \quad (1)$$

Here: L = distance between span, a = thickness of the composite, and D = diameter of the span.

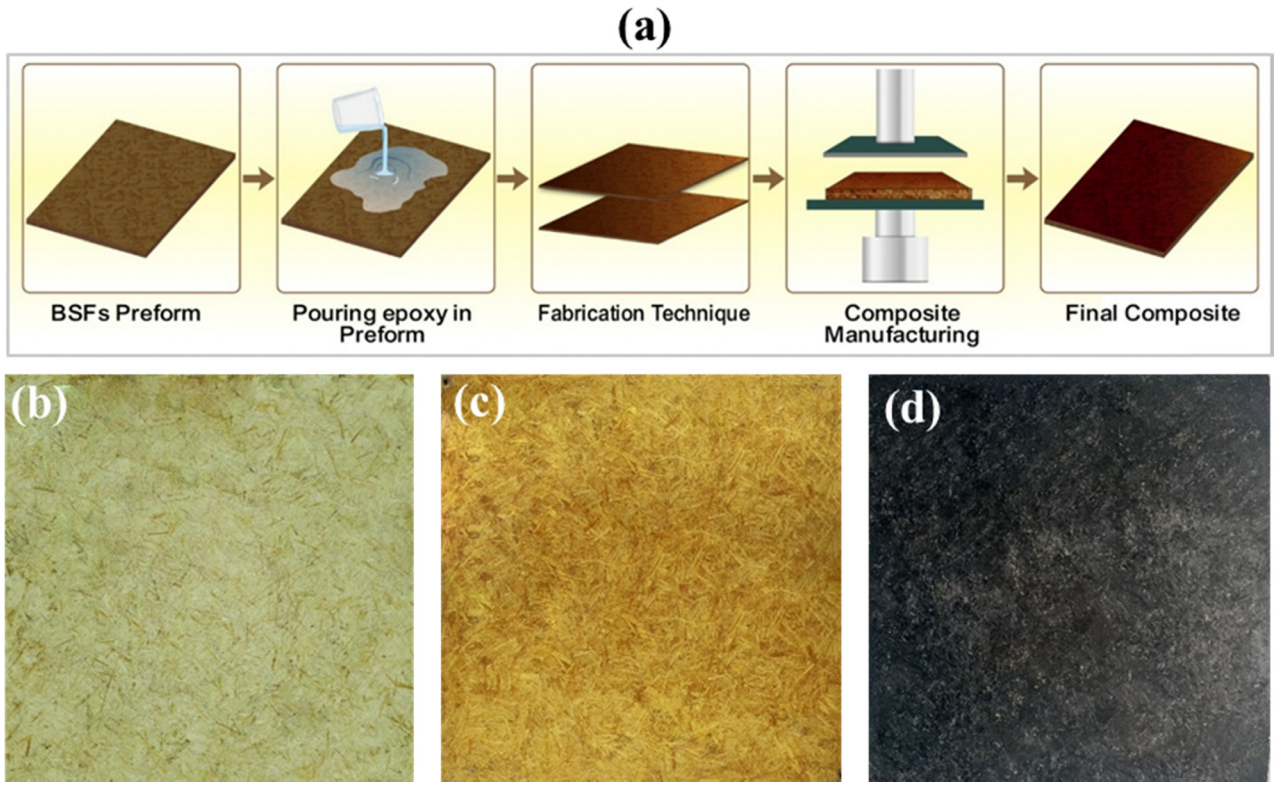

Fig. 5 BSFs composites (a) manufacturing process, (b) untreated composite, (c) alkali-treated composite, and (d) GO-treated composite.

2.3.3. Impact test. Tests for impact resistance used a Charpy impact tester (Zwick Roell model) in compliance with ASTM D 256 standards. The test specimens, composed of 60 mm × 20 mm × 3 mm dimensions each, received a hammer strike to measure fracture energy absorption. The test calculated impact strength by dividing the total absorbed energy values by the area measurement of each specimen. Each type of composite material underwent room temperature testing, by which the average results from three specimens evaluated the toughness of the material alongside impact-induced failure resistance.

2.3.4. Hardness test. Shore durometer hardness (Shore-D) was used in this study to measure the surface hardness of the UTB5, UTB10, UTB15, UTB20, ATB, and AGB samples. The test was conducted according to the ASTM D2240 standard, with sample dimensions of 26 mm × 26 mm × 3 mm.

2.3.5. FTIR analysis. To examine the changes in the chemical structure of bamboo fibers after alkali treatment and GO coating, Fourier transform infrared (FTIR) spectroscopy was performed by dispersing powdered bamboo fiber composites in the machine, using an FTIR spectrometer (FTIR-4700, Italy). The spectra were recorded over a wave number range of 500–4000 cm^{-1}.

2.3.6. TGA analysis. Thermogravimetric analysis of the UTB5, ATB, and AGB samples was tested using a TA Instruments Q500. The samples, typically around 10 mg in weight, were heated in a nitrogen atmosphere at a constant rate of 10 °C min^{-1}, from room temperature to 800 °C. Mass loss was monitored as a function of temperature to identify degradation patterns and determine the temperature.

2.3.7. SEM study. Fractographic analysis of the fractured samples after tensile testing was conducted using a Phenom Pro-G desktop scanning electron microscope (SEM) from the Netherlands. All samples were coated with gold, and images were captured at several magnifications.

2.3.8. Dynamic mechanical analysis. The DMA of UTB5, ATB, and AGB composites was tested using a TA Q800 machine in the double cantilever bending mode, applying a frequency of 1 Hz and a temperature ramp of 2 °C min^{-1} from 30 °C to 150 °C. The DMA analysis provided the storage modulus, loss modulus, and damping factor (tan δ) properties.

2.3.9. Water absorbency test. The hybridized composite water absorption was measured according to ASTM D570-99 standards. The slicing process produced three specimen pieces from each composite, ranging between lengths of 39 mm and widths of 10 mm. Resin application, followed by curing, occurred on the selvages to block water entry. A precision balance measured the dried weight (W_i) of the samples once they reached 105 °C for at least one hour. Researchers submerged specimens in water at 23 °C (room temperature) for 30 days. The specimens underwent an additional weighing procedure (W_f) after tissue paper was wiped over them to remove residual water. The calculation of water absorption followed the formula shown in eqn (2).

$$\text{Water uptake}\,(\%) = \frac{W_f - W_i}{W_f} \times 100 \quad (2)$$

3. Results and discussions

3.1. Physical properties of composites

The physical properties of the several composites (see Table 4) were significantly influenced by the fiber length and the treatments applied. The volume fraction of fibers (FvF) in the composites confirmed variation based on the treatment and fiber length. The untreated raw bamboo composites (UTB5, UTB10, UTB15, UTB20) showed a relatively low fiber volume fraction, ranging from 38.9% to 44.17%, which aligns with the findings of a former study.[67,68] The FvF in these composites was largely influenced by the inherent characteristics of the bamboo fibers, which include impurities like hemicellulose, lignin, and wax. These impurities cramped the optimal packing of fibers, resulting in lower fiber content of the composites.

After the alkali treatment (ATB) was applied to the fibers (5 mm length fibers), the fiber volume fraction increased significantly to 47.35%. This treatment is typically used to remove impurities and improve fiber cleanliness, and plays a major role in enhancing the packing of fibers in the composite. The alkali treatment excellently increased the surface roughness and bonding potential of the fibers, allowing for a higher volume fraction and better interaction between the fibers and matrix. This result aligns with findings from previous studies,[69,70] where alkali treatment improved fiber–matrix bonding and increased FvF. When the ATB were dip-coated in a 1 wt% GO solution (AGB), the volume fraction of fibers in the AGB composite was 46.14%, slightly lower than that of the ATB composite but still showing a marked improvement over the untreated composites. For the GO coating, the FvF of the AGB composite was decreased.

The physical property results suggest that while the fiber length does not substantially affect the fiber volume fraction in

Table 4 Measured and calculated weight and volume fractions, densities, and void content of short bamboo fiber composites

Composite code	Weight of fibers (g)	Weight of composite (g)	Weight fraction of fibers (w_f)	Weight fraction of matrix (w_m)	Volume fraction of fibers (v_f)	Volume fraction of matrix (v_m)	Theoretical density of composite (g cm^{-3})	Experimental density of composite (g cm^{-3})	Void content (%)
UTB5	58.38	120.26	48.54	51.46	44.17	55.83	1.21	1.19	0.43
UTB10	56.36	119.23	47.27	52.73	41.81	58.19	1.19	1.18	0.55
UTB15	52.56	115.36	45.56	54.44	39.58	60.42	1.20	1.19	0.52
UTB20	51.65	116.62	44.29	55.71	38.9	61.42	1.19	1.17	0.64
ATB	59.12	114.25	51.74	48.26	47.35	52.65	1.22	1.20	0.33
AGB	65.15	125.32	51.98	48.02	46.14	53.86	1.23	1.20	0.38

raw bamboo fiber composites, the application of chemical treatments such as alkali treatment and the use of GO can significantly improve fiber packing and bonding within the composite, which reflects findings reported in previous literature.[71,72] These findings underscore the importance of chemical treatments in enhancing the properties of fiber-based composites.

3.2. Tensile properties

3.2.1. Effect of fiber lengths. The length of fibers plays a critical role in determining the tensile properties of fiber-reinforced composites. This is particularly important in natural fiber composites where factors such as fiber alignment, matrix interaction, and fiber packing are key to achieving optimal mechanical performance. In this study, the tensile strength and modulus of composites made from different fiber lengths were evaluated, and the results are shown in Fig. 6. From the tensile strength data (see Fig. 6a), the composite with 5 mm long fibers (UTB5) exhibited the highest tensile strength of 65.58 MPa. The tensile strength gradually decreased with increasing fiber length, with UTB10, UTB15, and UTB20 composites showing lower strengths of 58.35 MPa, 53.73 MPa, and 44.36 MPa, respectively, which is similar to that observed in the previous study.[73,74] This tendency aligns with the general understanding that shorter fibers deliver better stress transfer due to their higher surface area and even distribution within the composite matrix. The shorter fibers (UTB5) generate better fiber–matrix bonding and a higher packing density. It leads to improved load transfer efficiency, ultimately resulting in higher tensile strength. The tensile modulus exhibited the same pattern, with UTB5 showing the highest modulus of 3.55 GPa (see Fig. 6b). The modulus regularly decreased as the fiber length increased, with UTB10, UTB15, and UTB20 showing values of 3.12 GPa, 2.54 GPa, and 1.85 GPa, respectively. The tensile modulus decreases when utilizing longer fibers because the aspect ratio decreases, thus lowering the fiber–matrix interaction and decreasing the load transfer throughout the fibers. A packed structure forms within the composite when fibers are shorter because of better material density and homogeneous distribution, which improves the stiffness.

Table 5 Tensile and flexural properties of short banana fiber composites

Composite code	Tensile strength (MPa)	Tensile modulus (GPa)	Flexural strength (MPa)	Flexural modulus (GPa)
UTB5	65.58 ± 3.12	3.55 ± 0.21	80.5 ± 3.26	5.52 ± 0.24
UTB10	58.35 ± 2.44	3.12 ± 0.23	73.83 ± 4.22	4.43 ± 0.31
UTB15	53.73 ± 3.31	2.54 ± 0.12	65.52 ± 3.89	4.13 ± 0.24
UTB20	44.36 ± 2.96	1.85 ± 0.2	58.13 ± 3.51	3.86 ± 0.19
ATB	83.58 ± 3.13	4.12 ± 0.18	93.35 ± 4.12	5.56 ± 0.28
AGB	140.23 ± 3.56	6.11 ± 0.22	155.62 ± 4.32	6.03 ± 0.33

3.2.2. Effects of chemical treatments. The application of treated bamboo composites created significant tensile properties (see Table 5), and these improvements were most pronounced in the 5 mm bamboo fiber (UTB5) composites, which previously demonstrated higher tensile strength and modulus results. In the case of the alkali treatment (ATB) and GO coating (AGB), the composites demonstrated a marked improvement in both tensile strength and modulus compared to the untreated fibers.

The tensile strength measurement for UTB5 composite materials revealed 65.58 MPa according to Fig. 6a. The tensile strength test following ATB alkali application on the composite rose to 83.58 MPa. Research indicates that the improvement level reaches approximately 27.4%. The removal of surface impurities through alkali treatment allows better bonding between fibers and matrix and results in enhanced mechanical properties. The maximum tensile strength appeared in the AGB composite with 140.23 MPa. The tensile strength of ATB composite increased to 140.23 MPa, which represented a 67.8% enhancement over that of ATB composite. The incorporation of GO probably increased the fiber-to-matrix bond because GO creates enhanced mechanical properties in composites because of its exceptional properties, including high surface area and strong bond formation capabilities, which had similarly been found in previous research.[73–76]

The tensile modulus showed similar trends in Fig. 6b. The UTB5 composite displayed a tensile modulus of 3.55 GPa while

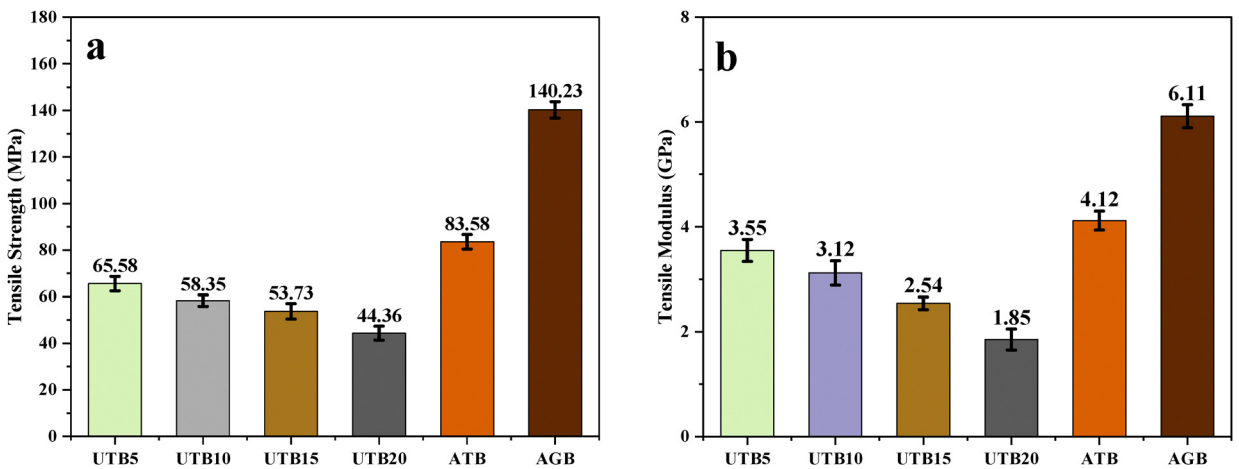

Fig. 6 Effect of fiber length and treatment on (a) tensile strength, and (b) tensile modulus of composites.

the ATB composite showed an increase to 4.12 GPa, a 16% improvement. The AGB composite had the highest tensile modulus at 6.11 GPa, marking a substantial improvement of almost 48% compared to UTB5. This growth in tensile modulus is compatible with the enhanced interfacial bonding and fiber–matrix interaction resulting from the alkali treatment and GO coating, which contribute to greater rigidity and resistance to deformation in the composite.

3.3. Flexural properties

3.3.1. Effect of fiber lengths. Fig. 7 shows that the effect of fiber length on the flexural properties of bamboo fiber composites was great, with shorter fibers showing better performance compared to longer fibers.[77] The flexural strength increased as the fiber length decreased, as shown in Fig. 7a. The UTB5 composite exhibited the highest flexural strength of 80.5 MPa, while the UTB10 composite showed a slightly lower strength of 73.83 MPa. The flexural strength continued to decrease for longer fibers. The UTB15 and UTB20 composites showed 65.52 MPa and 58.13 MPa of flexural strength, respectively. These results specify that shorter fibers lead to better overall composite performance.

In Fig. 7b, the improved flexural modulus observed in the UTB5 composite can be attributed to some factors. First, shorter fibers offer a greater surface area for bonding with the matrix. It leads to better interfacial adhesion and load transfer between the fibers and matrix. This allows for more effective stress distribution and improved flexural performance. Also, shorter fibers tend to have irregularities compared to longer fibers, which further contributes to the strength of the composite. Flexural stress is a combination of tensile and compressive stresses. In shorter fiber composites, the compressive waves can propagate more uniformly, resulting in more even stress distribution across the composite. On the other hand, longer fiber composites have a higher possibility of flaws and irregularities in the fibers, which can disrupt the uniformity of the compressive stress. This behavior aligns with findings from previous studies on natural fiber composites, which have shown that shorter fiber lengths generally result in better mechanical performance, as reported in previous work.[78]

3.3.2. Effects of chemical treatments. The flexural properties of bamboo fiber composites showed remarkable changes through chemical treatments (see Table 5). This improvement was observed in both flexural strength and modulus, as reported in previous work.[79] The raw, untreated 5 mm bamboo fiber composite (UTB5) exhibited a flexural strength of 80.5 MPa, as shown in Fig. 7a, which was the highest among the untreated fiber composites. After the application of alkali treatment (ATB), a notable increase in flexural strength of approximately 16% was observed. This enhancement in flexural strength can be attributed to the alkali treatment in removing impurities from the fiber surface, enhancing the surface roughness by breaking down the hydrogen bonds on the fiber surface. It improved the interfacial bonding between the fibers and the matrix and enhanced the load transfer capabilities of the composite. The most significant increase in flexural strength was observed in the AGB composite. The flexural strength of the AGB composite reached 155.62 MPa, representing a significant 66.7% development over the ATB composite. This result highlights the synergistic effect of GO on the composite properties. The oxygen-containing functional groups of GO can form strong bonds with alkali-treated fibers, enabling them to better transfer loads from the matrix, which aligns with prior data.[71,72,76]

Fig. 7b shows that the UTB5 composite had a flexural modulus of 5.52 GPa. The ATB composite showed an increase in flexural modulus to 5.56 GPa. The AGB composite showed the highest flexural modulus of 6.03 GPa, marking a 7.5% improvement over the alkali-treated composite. This growth can be attributed to the strong interfacial bonding formed by the GO coating, which enhances the overall stiffness and resistance to deformation of the composite.

3.4. Effect of fiber length and treatment on impact strength of composites

Impact strength is a parameter that shows the ability of a composite material to absorb energy upon impact (see Fig. 8a). It is faithfully related to the toughness of the composite. The relationship between fiber length, fiber loading, and

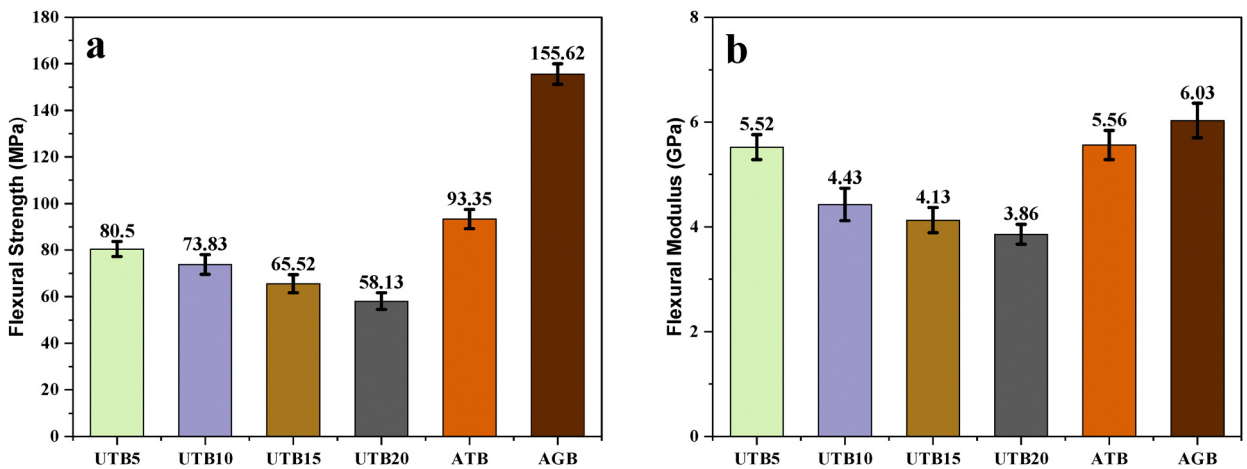

Fig. 7 Effect of fiber length and treatment on (a) flexural strength, and (b) flexural modulus of composites.

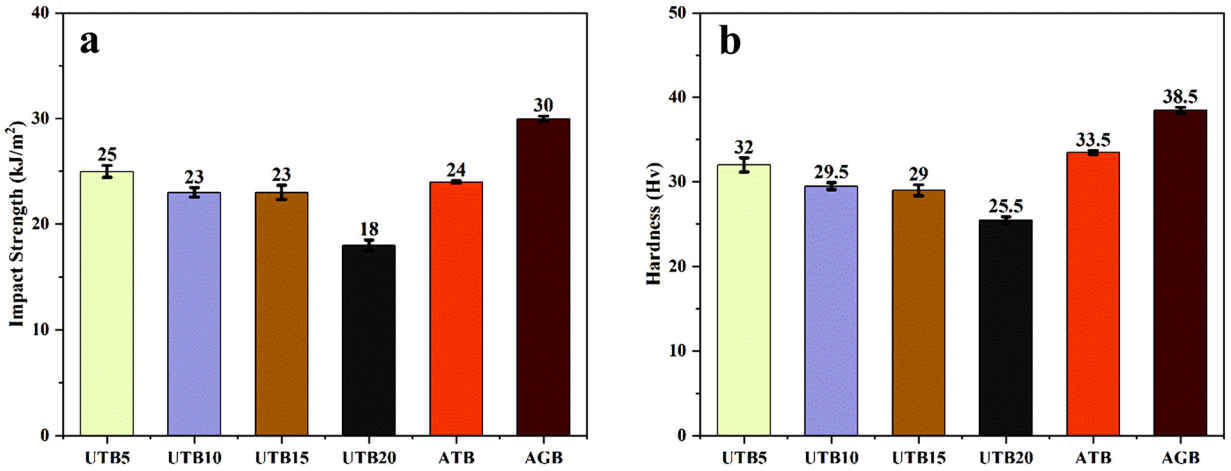

Fig. 8 Effect of fiber length and treatment on (a) impact strength, and (b) hardness test of composites.

impact strength is essential to understanding the overall performance of the material. The impact strength of the bamboo fiber composites varies based on both the fiber length and the chemical treatments applied to the fibers.

The UTB5 composite exhibited the highest impact strength of 25 kJ m^{-2}. This was higher than the composites made with longer fibers (UTB10, UTB15, and UTB20). The decrease in impact strength with increasing fiber length may be attributed to several factors. Longer fibers tend to create micro-spaces between the fiber and the matrix. This led to a less effective transfer of impact forces. These micro-spaces can serve as sites for crack initiation, reducing the capability to absorb energy and increasing the probability of crack propagation of the material. On the other hand, after treatment with alkali treatment (ATB) to the 5 mm bamboo fibers, the impact strength of the composite increased slightly to 24 kJ m^{-2}. The alkali treatment removed impurities and increased the bonding strength between the fibers and the matrix. The alkali treatment enhances energy absorption capacity and improves material toughness, aligning with prior data.[75,76] GO coating treatment produced the highest effect on impact strength in the AGB composite. It showed an impact strength of 30 kJ m^{-2}. The GO creates better bonding at fiber-to-matrix interfaces, resulting in the smooth transfer of loads while upgrading the energy dissipation during impact situations. This result recommends that the combination of chemical treatments not only enhances fiber–matrix bonding but also contributes to the overall toughness and impact resistance of the composite.

3.5. Effect of fiber length and treatment on hardness of composites

The hardness of a material refers to its capability to resist external deformation when subjected to an applied force. It is a crucial mechanical property for composites. It directly influences their performance under wear, abrasion, and indentation conditions. The effect of fiber length and chemical treatments on the hardness of bamboo fiber composites is shown in Fig. 8b.

The UTB5 composite exhibited the highest hardness value of 32 HV. This recommends that the shorter fiber length provides better reinforcement and surface strength in the composite, because of more uniform distribution of fiber. Fiber length was increased, and the hardness values slightly decreased. The UTB10, UTB15, and UTB20 composites displayed hardness values of 29.5 HV, 29 HV, and 25.5 HV, respectively. The decrease in hardness with increasing fiber length may be due to the creation of micro-spaces between the fibers and the matrix. Longer fibers tend to align less uniformly within the matrix, which reduces the overall hardness of the composite. The hardness level of 5 mm bamboo fibers was enhanced after subjecting them to alkali treatment, as reported in previous work.[80,81] The ATB composite measured 33.5 HV as its hardness. Alkali treatment makes composite material more rigid because it eliminates surface impurities. Testing revealed that the GO-coated composite (AGB) presented the maximum hardness of 38.5 HV. The hardening effect on the AGB composite originates from the combined treatment of alkali and GO.

3.6. FTIR analysis of composites

The Fourier Transform Infrared Spectroscopy (FTIR) spectra of the bamboo fiber composite (UTB5, ATB, and AGB) provide valuable insights into the functional groups present in the fibers. Also, give the effects of chemical treatments on their surface chemistry. The FTIR spectra showed significant changes in the functional groups of the fibers with different treatments (see Fig. 9).

The FTIR spectrum of UTB5 composite has a distinct peak at 3382 cm^{-1} representing the vibration stretch of O–H. The O–H stretching vibration at 3382 cm^{-1} is a common characteristic of cellulose in bamboo fibers. The C–H symmetrical stretching appears together with cellulose units in the fiber structure, which is shown in the 2900 cm^{-1} peak. C═O groups appear at 1745 cm^{-1} due to carbonyl bonds that typically exist within lignin and hemicellulose components. The peaks at 1617 cm^{-1} and 1316 cm^{-1} are linked to C═C aromatic stretching and C–O bond vibrations, respectively. It is confirmed that lignin and other non-cellulosic components are present in the untreated fiber. In the ATB composite, the C═O peak at 1745 cm^{-1} and

the C–O bond peak at 1316 cm^{-1} experience significant intensity reduction, similar to that observed in the previous study.[82] The decreased peak intensity reveals the successful removal of lignin and hemicellulose during treatment. The surface reactivity of the fibers increases after alkali treatment because the treatment removes both hemicellulose and lignin components from the natural fiber material. A new peak O═C═O and intensified C–O absorption became visible in the FTIR spectrum of the AGB composite when recorded at 2350 cm^{-1} and 1316 cm^{-1}, respectively. The data confirms that GO integration on the surface of the fiber exists successfully. The graph of intensities shows GO bonds to bamboo fiber oxygen groups, which strengthens fiber–matrix bonding. The presence of the characteristic GO peak at 2348 cm^{-1} is observed as O═C═O through FTIR spectral analysis, which was reported before.[82,83] The analysis verified that GO succeeded in modifying the fiber surface properties.

3.7. TGA analysis and DTG of composites

Fig. 10a shows the thermogravimetric analysis (TGA) curves. These provide valuable insights into the thermal degradation behavior of the bamboo fiber composites (UTB5, ATB, and AGB). TGA measures a weight loss of material as a temperature function, which indicates its thermal stability and decomposition characteristics.

The UTB5 composite showed a significant weight loss at around 200 °C to 380 °C. This temperature range is similar to the degradation of hemicellulose, cellulose, and lignin. The untreated fibers exhibit a rapid weight loss in this range, indicating lower thermal stability. When the temperature reaches around 400 °C, the composite has lost nearly 80% of its initial weight. This means that the thermal stability of the untreated bamboo fiber composite is poor. The ATB composite showed improved thermal stability compared to the UTB5 composite, as aligned with the previous article.[84] The weight loss in the ATB composite started at a slightly higher temperature, and the degradation rate was slower in the temperature range from 200 °C to 380 °C. This indicates that the alkali treatment has removed some non-cellulosic components, which can undergo thermal degradation. As a result, the ATB composite shows less weight loss in the critical degradation region. The AGB composite exhibited the highest thermal stability among the three composites, which agrees with a previous study.[85,86] The weight loss in the AGB composite started at a higher temperature and proceeded more slowly than in the UTB5 and ATB composites. The additional GO coating delivers better thermal stability to the ATB composite by improving fiber–matrix interaction and creating a stable physical structure that protects against thermal degradation.

From the DTG curves (see Fig. 10b), the UTB composite decomposes sooner compared to the treated composite. The delayed peak observed in the ATB composite indicates that alkali treatment has increased thermal stability. Significantly, the AGB composite demonstrates the most significance, with its major decomposition occurring at the highest temperature. The enhancement comes from the combined treatment with alkali and GO, which likely improves both the structure of the composite and its thermal capability of the composite.

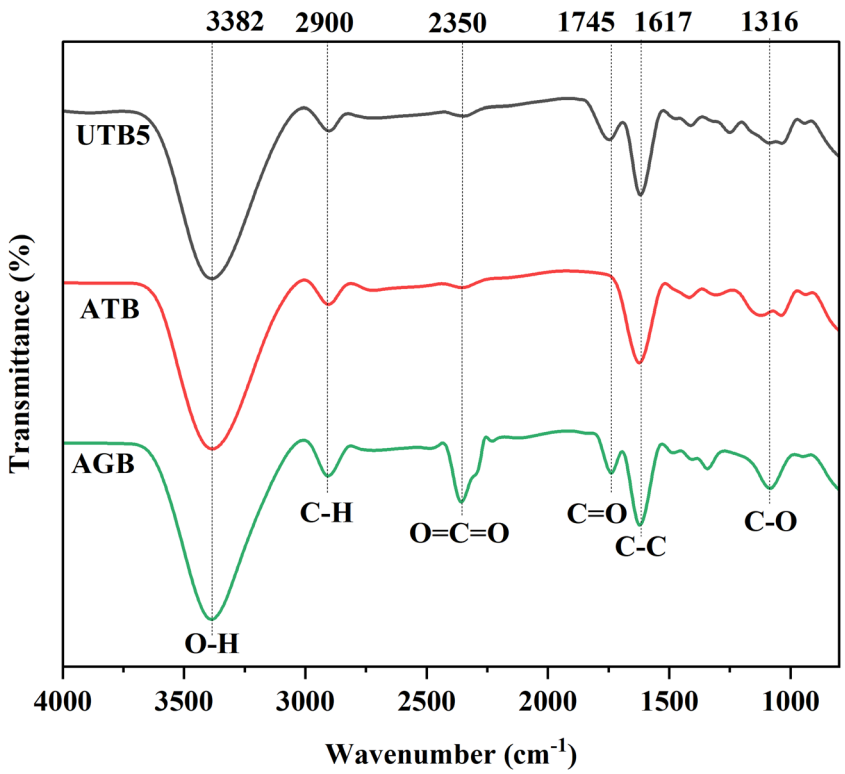

Fig. 9 FTIR analysis of untreated (UTB5), alkali-treated (ATB5), and GO-coated (AGB) composites.

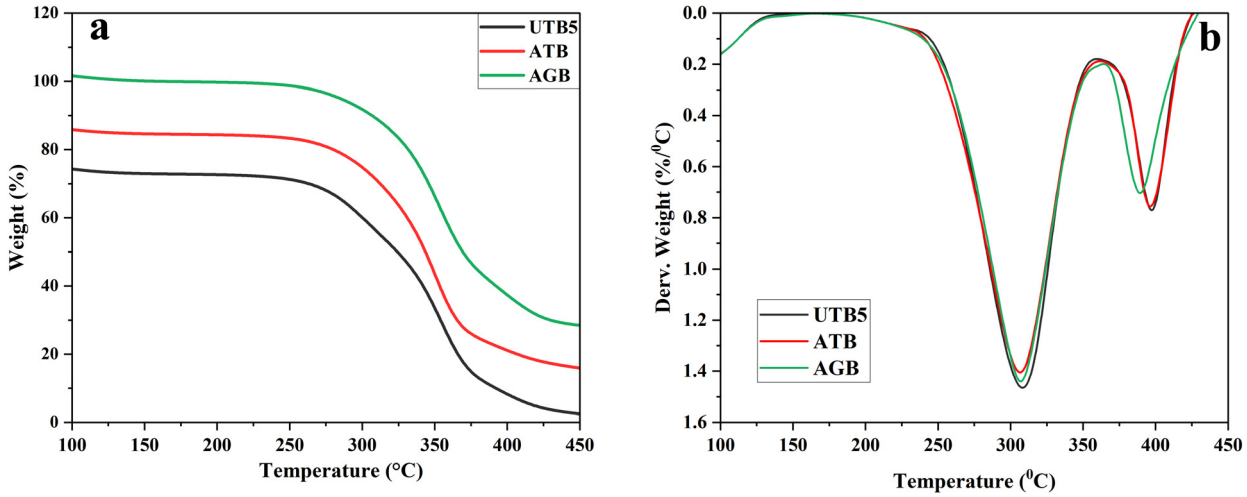

Fig. 10 (a) TGA analysis curves, and (b) DTG curve of composites.

3.8. SEM analysis

The SEM images in Fig. 11 comparatively illustrate the morphological changes and failure mechanisms in untreated (UTB5), alkali-treated (ATB), and GO-coated bamboo fiber composites (AGB) after tensile testing. In Fig. 11a, corresponding to the UTB5 composite, extensive fiber pull-outs and irregular fiber breakages are clearly observed (highlighted with red circles). These features indicate a weak fiber–matrix interface, leading to ineffective stress transfer during tensile loading. The heterogeneous structure and rough fracture surface suggest poor adhesion and are responsible for the lower mechanical strength of the UTB5 composite. Fig. 11b shows the morphology of the ATB composite. Alkali treatment has significantly reduced the amount of fiber pull-out, as highlighted, and fibers exhibit more linear and clean breakages. This change suggests that the removal of hemicellulose from the fiber surface enhanced interfacial bonding, improving load transfer efficiency between the fibers and the matrix. The improved adhesion led to a stronger and more cohesive fracture surface than the untreated sample. Further improvements are evident in Fig. 11c for the AGB composite, where alkali-treated bamboo fibers were coated with 1 wt% graphene oxide (GO). The presence of GO layers (indicated with arrows) on the fiber surfaces forms a uniform and continuous coating. This coating introduced additional oxygen-containing functional groups, facilitating strong chemical bonding with the matrix. As a result, the fracture surface appears highly compact with no noticeable fiber pull-outs and minimal fiber breakage. The improved fiber distribution, enhanced matrix bonding, and absence of interfacial defects indicate a significant increase in the mechanical performance of the composite, which was reported in previous work.[87]

3.9. Dynamic mechanical characterization

DMTA is a method to investigate the thermo-mechanical properties with the application of mechanical force, frequency, time, and temperature. The DMTA outcomes show mainly how stiff fiber-reinforced composites are and how well they crosslink and integrate fiber and matrix components, which are explained by terms like damping factor (tan δ), loss modulus (e''), and storage modulus (e'). The DMA parameters of the material demonstrate its two capabilities to absorb heat energy that results in damping

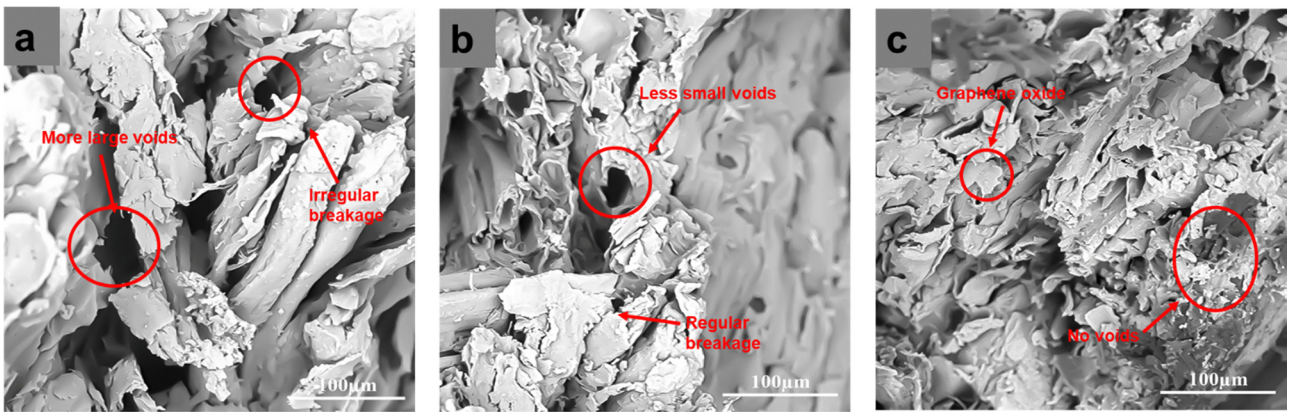

Fig. 11 SEM image of (a) UTB5, (b) ATB, and (c) AGB composites.

while maintaining its original shape upon removal of periodic stress forces.

3.9.1. Storage modulus. The data shown in Fig. 12a illustrates the changes in the storage modulus (E') of the composites as a function of temperature, ranging from 30 °C to 150 °C. The storage modulus of the composites decreased with increasing temperature. It is a common characteristic of polymer-based composites. Temperature elevation induces polymer chain relaxation in the matrix, thus lowering the material stiffness. A quick decline in storage modulus values occurred between 60 °C and 80 °C, which represents the glass transition zone of the matrix material. During the glass transition temperature (T_g), the polymer changes from its rigid glassy state to its flexible rubbery state, and this transition is characterized by a substantial decrease in storage modulus value. The storage modulus for the untreated 5 mm bamboo fiber composite (UTB5) reached its peak value of 9000 MPa in the temperature range. Both alkali-treated (ATB) and GO-coated (AGB) composites decreased in storage modulus values but maintained slightly higher values than the UTB5 composite during the temperature increase. The storage modulus from ATB powder composites reached 8000 MPa, yet the AGB powder composites demonstrated higher stiffness when their measurements yielded 8500 MPa. Alkali treatment and GO coating implemented separate effects on storage modulus values among untreated and treated composites. Treatment with alkali removes surface impurities, resulting in enhanced bonding between fiber and matrix, improving the composite mechanical properties and increasing storage modulus values, which agrees with a previous study.[88,89] The storage modulus of the AGB composites reached its maximum value at higher temperatures, becoming the highest among the treated composites after receiving the GO treatment. The additional GO interaction with bamboo fibers produces enhanced fiber–matrix connection, which drives improved mechanical properties.

3.9.2. Loss modulus. The loss modulus (E'') measures the ability of the material to absorb and dissipate mechanical energy, which indicates its damping behavior. As shown in Fig. 12b, the loss modulus curves of the bamboo fiber composites UTB5, ATB, and AGB demonstrate significant differences in their energy dissipation capabilities as a function of temperature.

The loss modulus peak detected between 60 °C and 90 °C in all composites matched exactly with the glass transition region of the epoxy matrix. The material undergoes a stiffness change between rigid and flexible states, leading to a strong increase in energy loss. After the peak point, the material achieves its lowest loss modulus rate because it continues into the polymer chain flexible rubbery plateau. The intrinsic peak loss modulus value found for the untreated 5 mm bamboo fiber composite reached 800 MPa, indicating a standard energy dissipation ability. The peak loss modulus value for the ATB and AGB composites exceeded 800 MPa because these composites demonstrated peak loss modulus values at 900 MPa and 1000 MPa, respectively, as reported in previous work.[89] The energy dissipation capacity of composites is improved through chemical treatments, which result in higher peak loss modulus values. The enhanced fiber–matrix interaction caused by alkali treatment and GO coating increases the loss modulus value. Alkali treatment creates a purification effect that strengthens the bond between the fiber and matrix, which increases the mechanical energy absorption capacities of the composite. The addition of GO coating enhances composite interfacial adhesion, which leads to better damping performance across the material. The highest loss modulus of the AGB composite predicts that it will demonstrate superior flexibility and impact resistance than the UTB5 composite. The application could benefit from such properties within structural composites, which have to withstand dynamic loading conditions because of improved damping and energy absorption.

3.9.3. Damping factor. The damping factor, known as tan δ, gives researchers information about the energy absorption ability of composite materials, polymeric chain movement, and their matrix-fiber interfacial relationships. The peak value of the glass transition temperature (T_g) of the composite material emerges from tan δ, which represents the ratio between loss modulus (E'') and storage modulus (E'). This value marks the temperature range during which the material transforms from inflexible to flexible state. The damping factor measuring the temperature-dependent behavior displays separate patterns among bamboo composites UTB5, ATB, and AGB when studied under Fig. 12c. All composites displayed an increase in tan δ while temperature rose until it reached 90 °C, where the peak

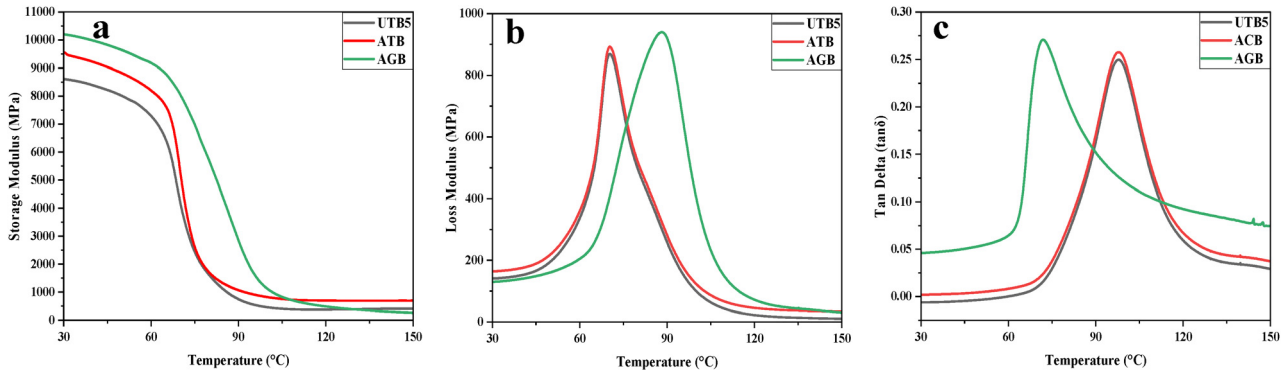

Fig. 12 DMA analysis of untreated (UTB5), alkali-treated (ATB), and GO-coated (AGB) composites at a wide range of temperatures (a) storage modulus (MPa), (b) loss modulus (MPa), and (c) tan delta (tan δ) curves.

occurred, matching the glass transition temperature of epoxy. The tan δ values descended after the peak temperature, corresponding to the rubbery region when the polymer chains became loose and used less energy for dissipation. The tan δ peak in UTB5 remained small, indicating decreased energy dissipation compared to samples with further treatment. The energy-absorption and dissipation properties of UTB5 material show a peak tan δ level at 0.1, thus indicating moderate performance. The peak tan δ measurement for ATB reached about 0.15, hence demonstrating better energy absorption in the material. Better fiber–matrix interaction from alkali treatment enhances the viscoelastic behavior of the composite because it leads to higher tan δ value in the ATB composite. When compared to the other composites, the GO-coated composite (AGB) displayed the highest peak tan δ value at 0.25. Energy dissipation capacity of the AGB composite increases because GO addition helps the material achieve better damping factor performance. The unique bonding characteristics of GO improve fiber–matrix interactions because they enhance energy absorption combined with structural flexibility. The data from tan δ measurements delivers valuable information regarding the mechanical traits of the material. The ductility of critical applications that demand energy dissipation benefits from higher damping factor values because they enable flexible materials that can absorb impacts. The superior damping factor of AGB composite is recommended for such applications since it would outperform UTB5 composite performance, as aligned with the previous article.[90]

3.10. Water absorption behavior of the composites

Bamboo fiber composites require assessment of how they absorb water before being suitable for applications that experience moisture or wetness. The water absorption data show that all bamboo fiber composites, including UTB5, UTB10, UTB15, UTB20, ATB, and AGB, demonstrate Fickian behavior, which results in time-dependent increasing water absorption until reaching saturation (see Fig. 13).

The untreated bamboo composites with 5 mm fiber length (UTB5) demonstrated the minimum water absorption at 5% during 50 hours immersion period. The water absorption amount increased across the board as the length of fibers grew longer from the 10 mm (UTB10) to the 15 mm (UTB15) and 20 mm (UTB20) composite types. After the testing period ended, the UTB10, UTB15, and UTB20 composite materials achieved water absorption levels reaching 5%, 4.5%, and 4%. The extended fibers in the composite allowed additional water absorption because they presented higher surface area combined with better hydrophilic properties that facilitate moistening over time. The placements of water molecules onto fibers are enhanced when fibers extend due to better water penetration potential. The alkali treatment on the composite material (ATB) produced well-regulated water absorption. From the first hours, the AT composite displayed increased water absorption until it reached stability at 3%. After alkali treatment, the fiber–matrix bond improves because removing lignin and hemicellulose from the fiber surfaces enables enhanced chemical interaction. The surface of alkali-treated fibers contains more

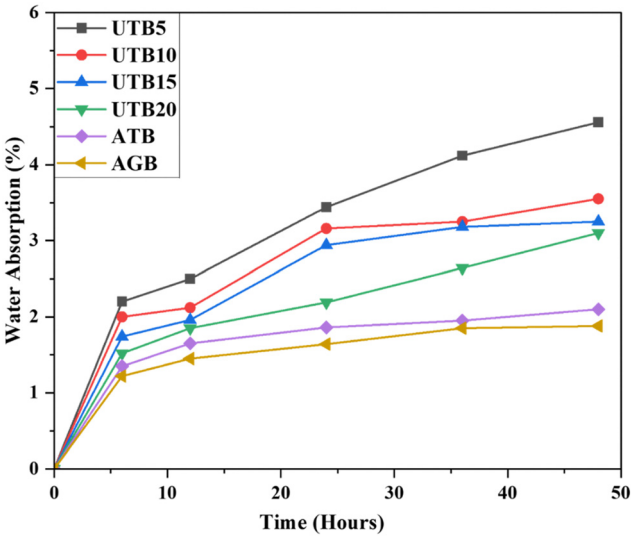

Fig. 13 Water absorption behavior of untreated, alkali-treated, and GO-coated composites.

hydrophilic sites after treatment, which temporarily absorb higher amounts of water than untreated familiar fibers during the early stages of water exposure. Water absorption levels from the GO-coated composite (AGB) exhibited the most intriguing results of all test groups. The addition of AGB in the composite material resulted in the lowest possible water retention, reaching equilibrium at 2% after 50 hours, which is in agreement with a previous study.[87,91,92] GO coating lowers water absorption because its hydrophobic nature creates a protective barrier that stops water from penetrating the fiber surface. The coating enhances the fiber–matrix bond, while the hydrophilic sites on fiber surfaces experience lower visibility, which results in better water resistance.

4. Conclusions

This study demonstrates the mechanical performance of epoxy composites reinforced with untreated and treated bamboo short fibers. The untreated bamboo fiber composites (UTB series) exhibited a decreasing trend in tensile and flexural properties with increasing fiber length. The highest mechanical performance was observed for UTB5. UTB5 achieved a tensile strength of 65.58 MPa and a flexural strength of 80.5 MPa. In comparison, the treated bamboo composite (ATB) demonstrated improved tensile strength of 83.58 MPa and flexural strength of 93.35 MPa. It indicates that alkali treatment effectively enhanced fiber–matrix bonding. Further improvement was achieved with composites by GO-coated bamboo fibers (AGB). It exhibited superior tensile strength (140.23 MPa) and flexural strength (155.62 MPa). The observed improvements are attributed to the improved interfacial bonding facilitated by graphene coating and alkali treatment. The improvement in mechanical properties suggests that graphene-coated bamboo fiber composites have promising potential for structural applications where lightweight and eco-friendly materials are required, such as automotive body parts,

and construction materials, *etc.* Future research should explore the optimization of treatment parameters and graphene loading, as well as their impact on fracture toughness and thermal properties. These findings contribute to the ongoing efforts to develop sustainable alternatives to synthetic fiber-reinforced composites for applications in aerospace, aircraft, automotive, construction, and household sectors.

Author contributions

Conceptualization: M. A. I., and M. I.; experimental design: M. A. I., M. I., M. S. I., and T. I.; methodology: M. A. I., M. I., M. S. I., and T. I.; material preparation M. A. I., M. I., M. S. I.; investigation: M. A. I., and T. I.; data curation: M. A. I., M. I., and M. S. I.; formal analysis: M. A. I., M. I., M. S. I., and T. I.; visualization: M. A. I., and T. I.; validation: M. A. I., and T. I.; supervision: M. A. I., and T. I.; original draft writing: M. A. I., M. I., M. S. I., and T. I.; writing – reviewing and editing: M. A. I., M. I., M. S. I., and T. I. All authors revised and approved the final manuscript.

Data availability

The authors verified that all included data met the dataset requirements. Supplementary details and explanations are available upon request from the corresponding authors.

Conflicts of interest

The authors declare no competing financial interest.

Acknowledgements

The authors did not receive any internal or external funding for the research. The authors would like to thank the Department of Textile Engineering and the Institute of Energy Engineering at Dhaka University of Engineering and Technology, Bangladesh, for providing laboratory facilities. The authors also acknowledge the Department of Textile Engineering, Jashore University of Science and Technology, Bangladesh, for providing technical support.

References

1 R. Siakeng, M. Jawaid, H. Ariffin, S. M. Sapuan, M. Asim and N. Saba, *Polym. Compos.*, 2019, **40**, 446–463.
2 M. D. Reale Batista, L. T. Drzal, A. Kiziltas and D. Mielewski, *Polym. Compos.*, 2020, **41**, 1074–1089.
3 H. Banga, V. K. Singh and S. K. Choudhary, *Innov. Syst. Des. Eng.*, 2025, **6**, 84–98.
4 D. E. C. Depuydt, N. Sweygers, L. Appels, J. Ivens and A. W. van Vuure, *J. Reinf. Plast. Compos.*, 2019, **38**, 397–412.
5 Z. Lou, Z. Zheng, N. Yan, X. Jiang, X. Zhang, S. Chen, R. Xu, C. Liu and L. Xu, *Forests*, 2023, **14**, 2266.
6 P. Zakikhani, R. Zahari, M. T. H. Sultan and D. L. Majid, *Mater. Des.*, 2014, **63**, 820–828.
7 P. Zakikhani, R. Zahari, M. T. H. Sultan and D. L. Majid, *Mater. Des.*, 2014, **63**, 820–828.
8 Y. A. Akinbade, Doctoral Dissertation, University of Pittsburgh (Unpublished), 2020, pp. 1–231.
9 F. Rusch, A. D. Wastowski, T. S. de Lira, K. C. C. S. R. Moreira and D. de Moraes Lúcio, *Biomass. Convers. Biorefin.*, 2023, **13**, 2487–2495.
10 L. Nayak and S. P. Mishra, *Fashion Textiles*, 2016, **3**, 1–23.
11 X. Wang, H. Ren, B. Zhang, B. Fei and I. Burgert, *J. R. Soc. Interface*, 2012, **9**, 988–996.
12 H. P. S. Abdul Khalil, I. U. H. Bhat, M. Jawaid, A. Zaidon, D. Hermawan and Y. S. Hadi, *Mater. Des.*, 2012, **42**, 353–368.
13 H. Bisheh, *Structures*, 2023, **54**, 198–220.
14 A. Muhammad, M. R. Rahman, S. Hamdan and K. Sanaullah, *Polym. Bull.*, 2019, **76**, 2655–2682.
15 A. Muhammad, M. R. Rahman, S. Hamdan and K. Sanaullah, *Polym. Bull.*, 2019, **76**, 2655–2682.
16 S. R. Mousavi, M. H. Zamani, S. Estaji, M. I. Tayouri, M. Arjmand, S. H. Jafari, S. Nouranian and H. A. Khonakdar, *J. Mater. Sci.*, 2022, **57**, 3143–3167.
17 M. Yang, W. Sun and W. Li, *Compos. Commun.*, 2023, **40**, 101598.
18 H. P. S. Abdul Khalil, I. U. H. Bhat, M. Jawaid, A. Zaidon, D. Hermawan and Y. S. Hadi, *Mater. Des.*, 2012, **42**, 353–368.
19 M. D. Reale Batista and L. T. Drzal, *Compos. Sci. Technol.*, 2018, **164**, 274–281.
20 M. M. E. Costa, S. L. S. Melo, J. V. M. Santos, E. A. Araújo, G. P. Cunha, E. P. Deus and N. Schmitt, *Procedia Eng.*, 2017, **200**, 457–464.
21 S. Özen, A. Benlioğlu, A. Mardani, Y. Altın and A. Bedeloğlu, *Constr. Build. Mater.*, 2024, **448**, 138225.
22 F. Gauvin, C. Richard and M. Robert, *Polym. Compos.*, 2018, **39**, 1534–1542.
23 O. Adekomaya and T. Majozi, *Int. J. Adv. Des. Manuf. Technol.*, 2019, **105**, 3183–3195.
24 J. Cruz and R. Fangueiro, *Procedia Eng.*, 2016, **155**, 285–288.
25 M. A. Rashid, J. H. Emon, M. A. Islam and M. N. Hasan, *ACS Appl. Polym. Mater.*, 2024, **6**, 9312–9322.
26 M. A. Rashid, M. A. Islam, M. N. Hasan, M. N. N. Anu and M. H. Ikbal, *Polym. Degrad. Stab.*, 2024, **229**, 110980.
27 R. de, S. Castoldi, L. M. S. de Souza, F. Souto, M. Liebscher, V. Mechtcherine and F. de Andrade Silva, *Constr. Build. Mater.*, 2022, **345**, 128363.
28 A. Roy, S. Chakraborty, S. P. Kundu, R. K. Basak, S. Basu Majumder and B. Adhikari, *Bioresour. Technol.*, 2012, **107**, 222–228.
29 M. I. Ibrahim, M. Z. Hassan, R. Dolah, M. Zuhri, M. Yusoff and S. Salit, *Malays. J. Fundam. Appl. Sci.*, 2018, **14**, 437–439.
30 M. R. Karim, S. Hasan, M. A. Islam, M. S. Uddin, M. A. Salam and M. Zakaria, *Biopolymers*, 2025, **116**, e23653.
31 V. Kaur, D. P. Chattopadhyay, S. Kaur and K. Kaur, *J. Text Sci. Eng.*, 2018, **8**, 1000362.
32 A. Roy, S. Chakraborty, S. P. Kundu, R. K. Basak, S. Basu Majumder and B. Adhikari, *Bioresour. Technol.*, 2012, **107**, 222–228.

33 M. M. E. Costa, S. L. S. Melo, J. V. M. Santos, E. A. Araújo, G. P. Cunha, E. P. Deus and N. Schmitt, *Proc. Eng.*, 2017, **200**, 457–464.
34 J. H. Emon, M. A. Rashid, M. A. Islam, M. N. Hasan and M. K. Patoary, *Reactions*, 2023, **4**, 737–765.
35 S. H. Mahmud, S. C. Das, A. Saha, T. Islam, D. Paul, M. W. Akram, M. S. Jahan, M. Z. I. Mollah, M. A. Gafur and R. A. Khan, *Next Sustainability*, 2025, **6**, 100104.
36 T. Islam, M. H. Chaion, M. A. Jalil, A. S. Rafi, F. Mushtari, A. K. Dhar and S. Hossain, *SPE Polym.*, 2024, **5**, 481–506.
37 G. Jena and J. Philip, *Prog. Org. Coat.*, 2022, **173**, 107208.
38 S. S. A. Kumar, S. Bashir, K. Ramesh and S. Ramesh, *Prog. Org. Coat.*, 2021, **154**, 106215.
39 S. Pei and H. M. Cheng, *Carbon*, 2012, **50**, 3210–3228.
40 J. I. Paredes, S. Villar-Rodil, A. Martínez-Alonso and J. M. D. Tascón, *Langmuir*, 2008, **24**, 10560–10564.
41 S. Stankovich, D. A. Dikin, R. D. Piner, K. A. Kohlhaas, A. Kleinhammes, Y. Jia, Y. Wu, S. B. T. Nguyen and R. S. Ruoff, *Carbon*, 2007, **45**, 1558–1565.
42 D. A. Dikin, S. Stankovich, E. J. Zimney, R. D. Piner, G. H. B. Dommett, G. Evmenenko, S. T. Nguyen and R. S. Ruoff, *Nature*, 2007, **448**, 457–460.
43 D. R. Dreyer, S. Park, C. W. Bielawski and R. S. Ruoff, *Chem. Soc. Rev.*, 2009, **39**, 228–240.
44 Y. Zhu, S. Murali, W. Cai, X. Li, J. W. Suk, J. R. Potts and R. S. Ruoff, *Adv. Mater.*, 2010, **22**, 3906–3924.
45 P. Bari, S. Khan, J. Njuguna and S. Mishra, *Int. J. Plast. Technol.*, 2017, **21**, 194–208.
46 A. H. Chisty, A. K. Mallik, F. N. Robel, M. Shahruzzaman, P. Haque, K. S. Hossain, R. A. Khan and M. M. Rahman, *ChemistrySelect*, 2019, **4**, 11417–11425.
47 W. Pang, Z. Ni, G. Chen, G. Huang, H. Huang and Y. Zhao, *RSC Adv.*, 2015, **5**, 63063–63072.
48 J. Liang, Y. Huang, L. Zhang, Y. Wang, Y. Ma, T. Cuo and Y. Chen, *Adv. Funct. Mater.*, 2009, **19**, 2297–2302.
49 Md. T. Hossain, S. Reza, Md. A. Islam, Md Mohebbullah and T. Islam, *ACS Appl. Eng. Mater.*, 2025, **3**, 1–20.
50 J. Chen, J. Wu, H. Ge, D. Zhao, C. Liu and X. Hong, *Composites, Part A*, 2016, **82**, 141–150.
51 P. Wang, J. Yang, W. Liu, X. Z. Tang, K. Zhao, X. Lu and S. Xu, *Mater. Des.*, 2017, **113**, 68–75.
52 M. R. Repon, T. Islam, T. Islam and M. A. Alim, *Plant Biomass Derived Materials: Sources, Extractions, and Applications*, 2024, pp. 363–388.
53 X. Zhang, X. Fan, C. Yan, H. Li, Y. Zhu, X. Li and L. Yu, *ACS Appl. Mater. Interfaces*, 2012, **4**, 1543–1552.
54 M. A. Rashid, M. Y. Ali, M. A. Islam and M. A. Kafi, *Ind. Crops Prod.*, 2025, **224**, 120303.
55 F. Li, Y. Liu, C. B. Qu, H. M. Xiao, Y. Hua, G. X. Sui and S. Y. Fu, *Polymer*, 2015, **59**, 155–165.
56 X. J. Shen, L. X. Meng, Z. Y. Yan, C. J. Sun, Y. H. Ji, H. M. Xiao and S. Y. Fu, *Composites, Part B*, 2015, **73**, 126–131.
57 J. Chen, D. Zhao, X. Jin, C. Wang, D. Wang and H. Ge, *Compos. Sci. Technol.*, 2014, **97**, 41–45.
58 R. Xiong, A. M. Grant, R. Ma, S. Zhang and V. V. Tsukruk, *Mater. Sci. Eng., R*, 2018, **125**, 1–41.
59 R. Xiong, H. S. Kim, L. Zhang, V. F. Korolovych, S. Zhang, Y. G. Yingling and V. V. Tsukruk, *Angew. Chem., Int. Ed.*, 2018, **57**, 8508–8513.
60 R. Xiong, K. Hu, A. M. Grant, R. Ma, W. Xu, C. Lu, X. Zhang and V. V. Tsukruk, *Adv. Mater.*, 2016, **28**, 1501–1509.
61 M. R. Karim, S. Hasan, M. A. Islam, M. S. Uddin, M. A. Salam and M. Zakaria, *Biopolymers*, 2025, **116**, e23653.
62 H. Wang, G. Xian and H. Li, *Composites, Part A*, 2015, **76**, 172–180.
63 M. A. Arfaoui, P. I. Dolez, M. Dubé and E. David, *Appl. Surf. Sci.*, 2017, **397**, 19–29.
64 L. Shahriary and A. A. Athawale, *Graphene Oxide Synthesized by using Modified Hummers Approach*, 2014, vol. 02.
65 J. Kaima, I. Preechawuttipong, R. Peyroux, P. Jongchansitto and T. Kaima, *Res. Eng.*, 2023, **18**, 101186.
66 F. S. da Luz, F. da Costa Garcia Filho, M. T. G. del-Río, L. F. Cassiano Nascimento, W. A. Pinheiro and S. N. Monteiro, *Polymers*, 2020, **12**(7), 1601.
67 G. Coroller, A. Lefeuvre, A. Le Duigou, A. Bourmaud, G. Ausias, T. Gaudry and C. Baley, *Composites, Part A*, 2013, **51**, 62–70.
68 S. C. Chin, K. F. Tee, F. S. Tong, H. R. Ong and J. Gimbun, *Mater. Today Commun.*, 2020, **23**, 100876.
69 H. Chen, W. Zhang, X. Wang, H. Wang, Y. Wu, T. Zhong and B. Fei, *J. Wood Sci.*, 2018, **64**, 398–405.
70 T. T. L. Doan, H. Brodowsky and E. Mäder, *Compos. Sci. Technol.*, 2012, **72**, 1160–1166.
71 U. O. Costa, L. F. C. Nascimento, J. M. Garcia, S. N. Monteiro, F. S. da Luz, W. A. Pinheiro and F. da Costa Garcia Filho, *Polymers*, 2019, **11**, 1356.
72 F. S. da Luz, F. da Costa Garcia Filho, M. T. G. del-Río, L. F. Cassiano Nascimento, W. A. Pinheiro and S. N. Monteiro, *Polymers*, 2020, **12**, 1601.
73 A. C. Manalo, E. Wani, N. A. Zukarnain, W. Karunasena and K. T. Lau, *Composites, Part B*, 2015, **80**, 73–83.
74 K. Zhang, F. Wang, W. Liang, Z. Wang, Z. Duan and B. Yang, *Polymers*, 2018, **10**, 608.
75 M. A. Rafiee, J. Rafiee, Z. Wang, H. Song, Z. Z. Yu and N. Koratkar, *ACS Nano*, 2009, **3**, 3884–3890.
76 M. Tian, L. Qu, X. Zhang, K. Zhang, S. Zhu, X. Guo, G. Han, X. Tang and Y. Sun, *Carbohydr. Polym.*, 2014, **111**, 456–462.
77 A. Ashori, S. Sheshmani and F. Farhani, *Carbohydr. Polym.*, 2013, **92**, 865–871.
78 D. Bachtiar, S. M. Sapuan and M. M. Hamdan, *Mater. Des.*, 2008, **29**, 1285–1290.
79 W. Yao and Z. Li, *Cem. Concr. Res.*, 2003, **33**, 15–19.
80 S. S. Alam, M. R. Munshi, A. Shufian, M. M. Haque, M. R. Haque, M. Hasan, M. A. Gafur and F. Rahman, *Adv. Mater. Proc. Technol.*, 2024, **10**, 329–348.
81 R. A. Kurien, M. Maria Anil, S. L. Sharan Mohan and J. Anna Thomas, *Mater. Today Proc.*, 2023, DOI: **10.1016/j.matpr.2023.04.363**.
82 M. Das and D. Chakraborty, *J. Appl. Polym. Sci.*, 2006, **102**, 5050–5056.
83 A. M. Abdelkader and I. A. Kinloch, *ACS Sustainable Chem. Eng.*, 2016, **4**, 4465–4472.

84 X. Fang, J. Xu, H. Guo and Y. Liu, *Fibers Polym.*, 2023, **24**, 505–514.
85 J. Alongi and G. Malucelli, *Polym. Degrad. Stab.*, 2013, **98**, 1428–1438.
86 D. G. Papageorgiou, Z. Terzopoulou, A. Fina, F. Cuttica, G. Z. Papageorgiou, D. N. Bikiaris, K. Chrissafis, R. J. Young and I. A. Kinloch, *Compos. Sci. Technol.*, 2018, **156**, 95–102.
87 N. Venkateshwaran, A. Elayaperumal and M. S. Jagatheeshwaran, *J. Reinf. Plast. Compos.*, 2011, **30**, 1621–1627.
88 D. Kusić, U. Božič, M. Monzón, R. Paz and P. Bordón, *Materials*, 2020, **13**, 3581.
89 S. A. Paul, C. Sinturel, K. Joseph, G. D. G. Mathew, L. A. Pothan and S. Thomas, *Polym. Eng. Sci.*, 2010, **50**, 384–395.
90 L. A. Pothan, Z. Oommen and S. Thomas, *Compos. Sci. Technol.*, 2003, **63**, 283–293.
91 A. Balaji, S. Kannan, R. Purushothaman, S. Mohanakannan, A. H. Maideen, J. Swaminathan, B. Karthikeyan and P. Premkumar, *Biomass. Convers. Biorefin.*, 2024, **14**, 7835–7845.
92 K. Shahapurkar, G. Gebremaryam, G. Kanaginahal, S. Ramesh, N. N. Nik-Ghazali, V. Chenrayan, M. E. M. Soudagar, Y. Fouad and M. A. Kalam, *J. Nat. Fibers*, 2024, **21**, 2338930.